

## Original article

# Combination of sonic wave velocity, density and electrical resistivity for joint estimation of gas-hydrate reservoir parameters and their uncertainties

Xin Zhang<sup>1,2,3</sup>, Qingping Li<sup>4</sup>, Lixia Li<sup>4</sup>, Qi Fan<sup>4</sup>, Jianhua Geng<sup>1,2,3</sup>✉\*

<sup>1</sup>State Key Laboratory of Marine Geology, Tongji University, Shanghai 200092, P. R. China

<sup>2</sup>School of Ocean and Earth Science, Tongji University, Shanghai 200092, P. R. China

<sup>3</sup>Center for Marine Resources, Tongji University, Shanghai 20092, P. R. China

<sup>4</sup>State Key Laboratory of Offshore Natural Gas Hydrates, CNOOC, Beijing 100027, P. R. China

### Keywords:

Gas-hydrate saturation  
porosity  
Bayesian inversion  
uncertainty

### Cited as:

Zhang, X., Li, Q., Li, L., Fan, Q., Geng, J. Combination of sonic wave velocity, density and electrical resistivity for joint estimation of gas-hydrate reservoir parameters and their uncertainties.

Advances in Geo-Energy Research, 2023, 10(2): 133-140.

<https://doi.org/10.46690/ager.2023.11.07>

### Abstract:

Gas-hydrate saturation and porosity are the most crucial reservoir parameters for gas-hydrate resource assessment. Numerous academics have put forward elastic and electrical petrophysical models for calculating the saturation and porosity of gas-hydrate. However, owing to the limitations of a single petrophysical model, the estimation of gas-hydrate saturation and porosity using single elastic or electrical measurement data appears to be inconsistent and uncertain. In this study, the sonic wave velocity, density and resistivity well log data are combined with a Bayesian linear inversion method for the simultaneous estimation of gas-hydrate saturation and porosity. The sonic wave velocity, density and resistivity data of the Shenhu area in the South China Sea are used to estimate the gas-hydrate saturation and porosity. To validate the accuracy of this method, the estimation results are compared with the saturation obtained from pore water chemistry and porosity obtained from density logs. The well log data examples show that the joint estimation method not only provides a rapid estimation of the gas-hydrate reservoir parameters but also improves the accuracy of results and determines their uncertainty.

## 1. Introduction

Gas-hydrate (GH), which is widely distributed in deep marine sediments and permafrost zones, contains a large amount of carbon resources, which plays an important role in the global carbon cycle and the utilization of natural resources (Collett et al., 2015; Boswell et al., 2020). In the past three decades, the United States, Canada, China, and Japan have conducted geological, geophysical and geochemical surveys and tested the production of GH, covering marginal sea and permafrost zones (Yu et al., 2019). China has launched several projects for GH research and field surveys in the South China Sea (SCS) since 2000 and successfully tested the production

of GH in its northern continental slope in 2017 and 2020 (Li et al., 2018; Ye et al., 2020). Porosity and GH saturation are two critical parameters when applying the volumetric method for estimating the GH reservoir reserves (Trofimuk et al., 1975; Chong et al., 2016).

In the Shenhu area of the SCS, GH is mainly dispersed within silty and silty-clay sediments (Wang et al., 2014). It can generally be postulated that GH in this region predominantly exist in the form of pore-filling structures (Li et al., 2014). Because the pores of the formation are filled with water, GH or free gas, there is a significant density difference between the pore-filling phase and the grain density of the formation. Therefore, porosity changes have a significant effect on density

(Lawrence and David, 2015). However, the density of GH is close to that of water, and estimating the hydrate saturation using density logs will create considerable uncertainty (Brugada et al., 2010). Similarly, sonic velocity is highly sensitive to changes in the formation porosity (Mavko et al., 2020). Furthermore, the formation water within rock pores serves as the primary conducting medium, and the presence of GH in these pores can obstruct the pathways, leading to increased electrical resistivity. As a result, electrical resistivity exhibits heightened sensitivity to variations in GH saturation (Jin et al., 2020). Accordingly, sonic wave velocity and resistivity are often used to quantitatively estimate the GH reservoir parameters (Shankar and Riedel, 2011).

Many studies have been conducted on estimating porosity and saturation in porous media by utilizing velocity or density. Wyllie et al. (1956) presented a classical time-average velocity model. Lee et al. (1996) established a four-phase weighted equation for sonic wave velocity. These velocity models have been used to estimate GH saturation (Chand et al., 2004). Lee and Collett (2001) modified the Biot-Gassmann theory to propose a model for predicting the compression and shear wave velocities of gas-hydrate-bearing loose sediments; nevertheless, the determination of Biot coefficient in the model has been a consistent challenge. Additionally, the various distribution forms of GH, including pore-filling, coating grains, supporting matrix, and cement at the contacts, result in significant differences in the sonic wave velocity and electrical resistivity of GH reservoirs (Dvorkin et al., 1999; Chand et al., 2004; Dai et al., 2004). Helgerud et al. (1999) proposed an effective media model for predicting the velocity of unconsolidated reservoirs with different GH distributions in the pore space. However, for this model, data on the precise elastic modulus, porosity and density of the solid matrix of the GH reservoir are necessary.

Alternatively, Archie (1942) introduced a classical resistivity model to estimate the fluid saturation of pure sandstone and low-mud content sandstone. Archie's equation, however, is not applicable to formations with high clay content. As an empirical equation, several parameters such as  $a$ ,  $m$  and  $n$  (see Eq. (3)) within this equation often need to be determined by experimental measurements or petrophysical analysis using well log data. Inaccurate parameter values can lead to unpredictable outcomes when utilizing resistivity for prediction (Cai et al., 2017; Cook and Waite, 2018). Despite subsequent advancements, such as the Simandoux model (Simandoux, 1963), which accounts for clay content, the selection of parameters within the model can influence the accuracy of the estimation results. Consequently, the estimation of porosity and GH saturation based on sonic wave velocity, density or resistivity alone is unreliable.

In this study, to jointly estimate the formation porosity and GH saturation and to achieve a more precise estimation of both, the authors employ a Bayesian framework that integrates sonic wave velocity, density and resistivity well log data. The latter is taken to from the Shenhu region in the SCS to assess the viability and efficiency of this approach.

## 2. Method

### 2.1 Petrophysical models

Petrophysical models bridge the gap between the rock physical properties and the reservoir parameters (Bosch et al., 2010). An obvious increase in sonic wave velocity and resistivity is observed in hydrate-rich reservoirs; therefore, both elastic and electrical petrophysical models can effectively estimate the hydrate reservoir parameters. Despite employing a petrophysical model that accounts for the various forms of GH occurrence, uncertainties arise in estimating GH saturation and porosity due to the complex nature of GH presence within the reservoir when a single model is used. This study combines elastic and electrical petrophysical models to simultaneously estimate the saturation and porosity of the GH reservoir by combining the time-averaged equations of sonic wave velocity and density along with Archie's resistivity model under a Bayesian framework. This strategy is expected to improve the reliability and reduce the uncertainty in the inversion results. Considering the linear Bayesian inversion, linear petrophysical models of velocity, density and resistivity are applied.

#### 2.1.1 Sonic wave velocity and density models

If GH is part of the pore fluid, the sonic wave velocity  $V_p$  and density  $\rho$  of the gas-hydrate-bearing formation can be expressed by three-phase time-averaged linear equations (Lee et al., 1996):

$$\frac{1}{V_p} = \phi S_w \frac{1}{V_w} + \phi (1 - S_w) \frac{1}{V_h} + (1 - \phi) \frac{1}{V_m} \quad (1)$$

$$\rho = \phi S_w \rho_w + \phi (1 - S_w) \rho_h + (1 - \phi) \rho_m \quad (2)$$

where  $S_w$  denotes water saturation,  $\phi$  denotes porosity,  $V_w$  denotes water velocity,  $V_h$  denotes GH velocity,  $V_m$  denotes the grain velocity of the gas-hydrate-bearing formation,  $\rho_w$  denotes pore water density,  $\rho_h$  denotes the density of the GH, and  $\rho_m$  denotes the grain density of the gas-hydrate-bearing formation, which varies with mineral composition.

#### 2.1.2 Resistivity model

In this work, Archie's equation (Archie, 1942) serves as the resistivity model:

$$R_t = a R_w \phi^{-m} S_w^{-n} \quad (3)$$

where  $R_t$  and  $R_w$  represent the formation resistivity and the connate water resistivity, respectively;  $a$ ,  $m$  and  $n$  represent the lithological coefficient, cementation index and saturation index, respectively.

#### 2.1.3 Linear models

Eqs. (1)-(2) are linear, whereas Eq. (3) is nonlinear. To simultaneously use the velocity, density and resistivity equations for the linear inversion of the GH reservoir parameters, it is necessary to linearize Eq. (3). Eqs. (1)-(2) can be parameterized as the product of saturation and porosity ( $A = S_w \phi$ ), and porosity:

$$\frac{1}{V_p} - \frac{1}{V_m} = \left( \frac{1}{V_w} - \frac{1}{V_h} \right) A + \left( \frac{1}{V_h} - \frac{1}{V_m} \right) \phi \quad (4)$$

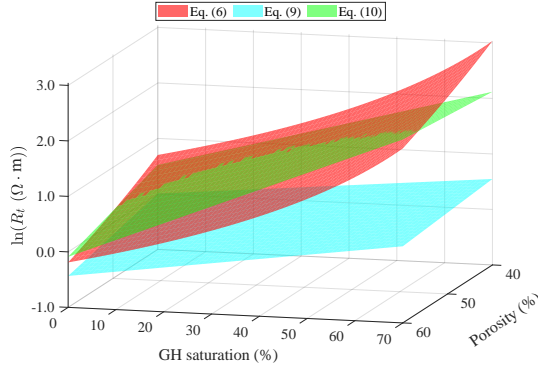


**Fig. 1.** Comparison of the original Archie's equation (red), linearized Archie's equation (blue) and optimized linearization of Archie's equation (green).

$$\rho - \rho_m = (\rho_w - \rho_h)A + (\rho_h - \rho_m)\phi \quad (5)$$

Taking the logarithms of both sides of Eq. (3) results in the expression:

$$\ln \frac{R_t}{aR_w} = -n \ln A + (n - m) \ln \phi \quad (6)$$

According to Taylor's expansion, as  $x$  approaches 0,  $\ln(1 + x) \approx x$ , so if  $A$  and  $\phi$  approach 1, the following equations are obtained:

$$\ln A = \ln(A - 1 + 1) \approx A - 1 \quad (7)$$

$$\ln \phi = \ln(\phi - 1 + 1) \approx \phi - 1 \quad (8)$$

Consequently, Eq. (6) can be rewritten as a linear expression:

$$\ln \frac{R_t}{aR_w} \approx n(1 - A) + (m - n)(1 - \phi) \quad (9)$$

Under normal conditions, the porosity of deep shallow sediment often ranges from 40% to 60% and even to 80% (Michelle et al., 2011). Thus, the assumption of  $\phi$  approaching 1 is basically satisfied, while the assumption of  $A$  approaching 1 is not satisfied. To mitigate the approximation of Eqs. (7) and (8), an introduction of two weighting coefficients,  $k_1$  and  $k_2$ , into Eq. (9) is performed, which results in:

$$\ln \frac{R_t}{aR_w} \approx k_1 n(1 - A) + k_2(m - n)(1 - \phi) \quad (10)$$

In order to determine the coefficients  $k_1$  and  $k_2$ , the initial application of the parameter values calculated by Kang et al. (2022) in Archie's equation is carried out, specifically,  $a = 1.12$ ,  $m = 2.22$ , and  $n = 1.9386$ . Subsequently, the range for porosity and GH saturation is established, and the computation of  $\ln R_t / (aR_w)$  according to Eq. (6) is conducted. Finally, the utilization of  $\ln R_t / (aR_w)$  in conjunction with Eq. (10) leads to the derivation of the values of  $k_1$  and  $k_2$  through the least squares method, resulting in the optimized coefficients of  $k_1 = 2.9409$  and  $k_2 = -10.0921$ . Fig. 1 illustrates the cross-plot of resistivity  $R_t$ , GH saturation  $S_{gh}$ , and porosity  $\phi$  calculated by Eqs. (6), (9), and (10), respectively. It can be observed that the linearized Eq. (10) provides a good approximation to Archie's original Eq. (6).

Eqs. (4), (5) and (10) make up a linear equation group,

which can be employed to simultaneously estimate the reservoir parameters of  $A$  and  $\phi$  using the sonic wave velocity, density and resistivity of well log data. After obtaining the two parameters of  $A$  and  $\phi$ , the  $S_{gh}$  can be calculated as  $S_{gh} = 1 - S_w$ .

## 2.2 Bayesian linear inversion

Eqs. (4), (5) and (10) can be written as:

$$d = GM \quad (11)$$

where  $d$ ,  $G$  and  $M$  represent observation data, forward operator and model parameters, respectively:

$$d = \begin{bmatrix} \frac{1}{V_p} - \frac{1}{V_m} \\ \rho - \rho_m \\ \ln \frac{R_t}{aR_w} - k_1 n - k_2(m - n) \end{bmatrix} \quad (12)$$

$$G = \begin{bmatrix} \frac{1}{V_w} - \frac{1}{V_h} & \frac{1}{V_h} - \frac{1}{V_m} \\ \rho_w - \rho_h & \rho_h - \rho_m \\ -k_1 n & k_2(n - m) \end{bmatrix} \quad (13)$$

$$M = \begin{bmatrix} A \\ \phi \end{bmatrix} \quad (14)$$

The maximum a posterior (MAP) solution of Eq. (11)  $\tilde{M}$  can be expressed as (Tarantola, 2005):

$$\tilde{M} = (G^T C_d^{-1} G + C_M^{-1})^{-1} (G^T C_d^{-1} d_{obs} + C_M^{-1} \mu_M) \quad (15)$$

where  $C_M$  denotes the covariance matrix of the model parameters,  $C_d$  denotes the covariance matrix of observation data,  $d_{obs}$  denotes observation data matrix, and  $\mu_M$  denotes the expectation matrix of model parameters.

The covariance matrix of the posterior probability density function (PDF)  $\tilde{C}_M$  is expressed as:

$$\tilde{C}_M = (G^T C_d^{-1} G + C_M^{-1})^{-1} \quad (16)$$

The variances of  $A$  and  $\phi$  can be obtained from the covariance matrix of the posterior model. Evidently,  $A$  and  $\phi$  are not independent. As a result, the posterior model standard deviation of saturation can only be obtained through a statistical proportional relationship between  $\phi$  and parameter  $A$ .

$$S_w(SD_{Post}) = A(SD_{Post}) \frac{S_w(SD_{Prior})}{A(SD_{Prior})} \quad (17)$$

where  $*(SD_{Post})$  denotes the standard deviation of the posterior model parameters, and  $*(SD_{Prior})$  denotes the standard deviation of the prior model parameters.  $S_w(SD_{Post})$  and  $\phi(SD_{Post})$  can be used to evaluate the uncertainty of the inversion results of GH saturation and porosity.

## 3. Calculation of real data

### 3.1 Well log data

The well log data utilized for estimating the GH reservoir gas hydrate saturation and porosity is sourced from well W19,

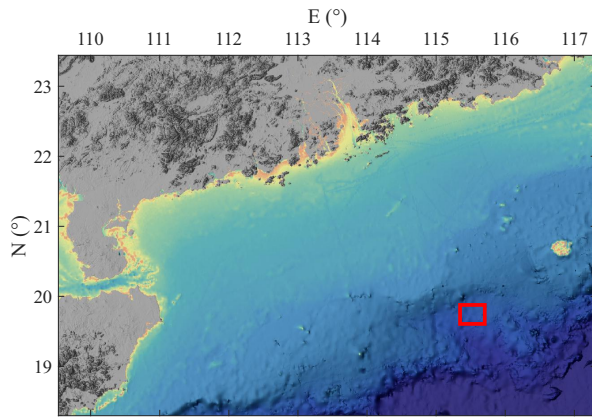


**Fig. 2.** Location of well W19 indicated by the red box.

situated within the Shenhu area in the SCS. This well, depicted in Fig. 2, is positioned at the center of the northern continental slope of the SCS (Yang et al., 2017). Fig. 3 displays the sonic P-wave velocity, density, resistivity, and density porosity curves (Sun et al., 2017; Qian et al., 2018; Kang et al., 2022). Previous studies have shown that well W19 has a gas-hydrate-bearing formation located at a depth of 1,410-1,444 meters (Yang et al., 2017) with the GH saturation estimated by the pore water chemistry, as shown in Fig. 3, which can be used as a reference for our inversion results.

### 3.2 Empirical parameters

The empirical parameters  $V_w$ ,  $V_h$ ,  $\rho_w$ ,  $\rho_h$ ,  $a$ ,  $m$ , and  $n$  in Eqs. (12)-(13) are given by referring to Kang et al. (2022), as shown in Table 1. Conversely, the grain velocity  $V_m$ , grain density  $\rho_m$ , and the connate water resistivity  $R_w$  of the gas-hydrate-bearing formation vary with the formation depth (Wood et al., 1994; Yun et al., 2005; Cai et al., 2017). Kang et al. (2022) discussed these parameters in detail when using data from well W19 to study GH saturation and porosity. In this paper, a thinner section of W19 is employed, allowing for the replacement of these parameters with the mean values calculated by Kang et al. (2022), as indicated in Table 1.

### 3.3 Inversion results

This study sets a step size of 12.5 meters to smooth the porosity curve derived from density logs and the GH saturation curve derived from pore water chemistry, resulting in prior models represented by the black dashed lines in Fig. 4. The GH saturation computed from the pore water chemistry and the porosity calculated from the density logs are used as reference values for evaluating the inversion results. The mean squared error (MSE) between the estimated values and the reference values, along with the covariance obtained from Bayesian inversion, is taken to assess the quality of joint inversion. Fig. 4 shows the MAP solutions of porosity and GH saturation and the covariance of posterior models. The estimated porosity curve is very close to that obtained from density logs, and its uncertainty is very small with a MSE of 0.0003 and mean standard deviation (MSD) of 0.0160. Similarly, the estimated GH saturation values closely resemble those calculated from pore water chemistry, with a MSE of 0.0196 and a MSD of

**Table 1.** The coefficients in Eq. (12).

$V_w$ (km/s)	$V_h$ (km/s)	$\rho_w$ (g/cm <sup>3</sup> )	$\rho_h$ (g/cm <sup>3</sup> )	$R_w$ ( $\Omega$ -m)
1.50	2.75	1.04	0.91	0.24
$V_m$ (km/s)	$\rho_m$ (g/cm <sup>3</sup> )	$a$	$m$	$n$
4.73	2.72	1.12	2.22	1.9386

**Table 2.** The coefficients in Eq. (12).

Prior model	$SD_{Prior}$	$SD_{Post}$	MSE
1	0.2353	0.0217	0.0235
2	0.4705	0.0284	0.1178
3	0.2673	0.0185	0.0202

0.0241.

As shown in Fig. 4, the MSE between the GH saturation calculated by the Simandoux model (Kang et al., 2022) and that calculated by pore water chemistry is 0.0478. The inversion result of the joint sonic wave velocity, density and resistivity is clearly more accurate than that of the single resistivity method.

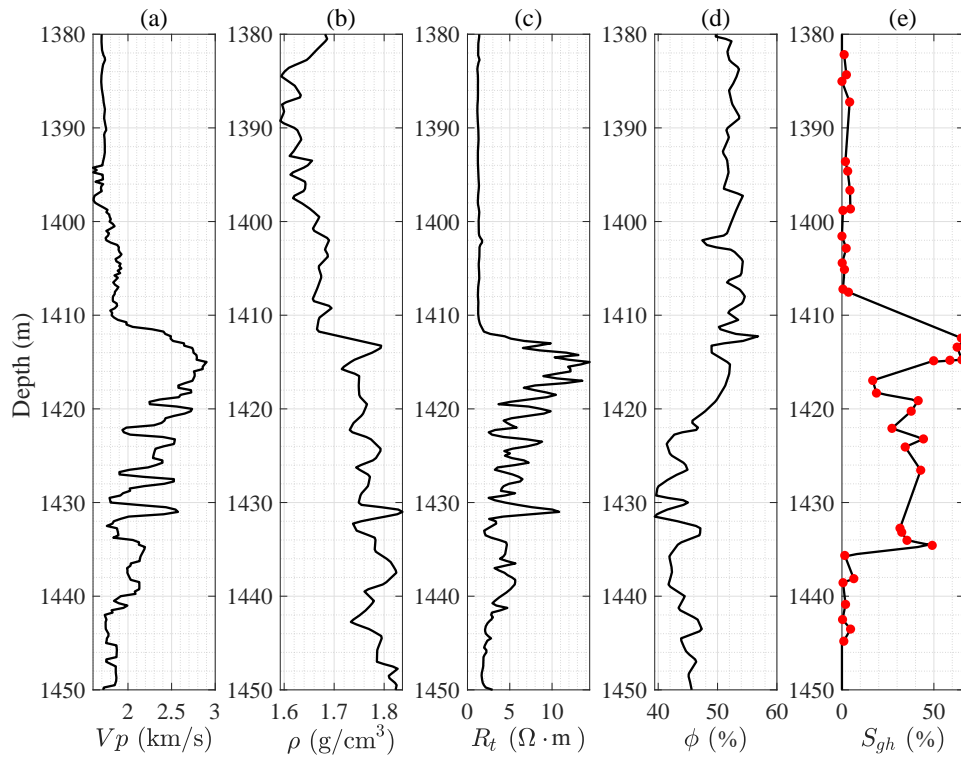
## 4. Discussion

### 4.1 Prior model

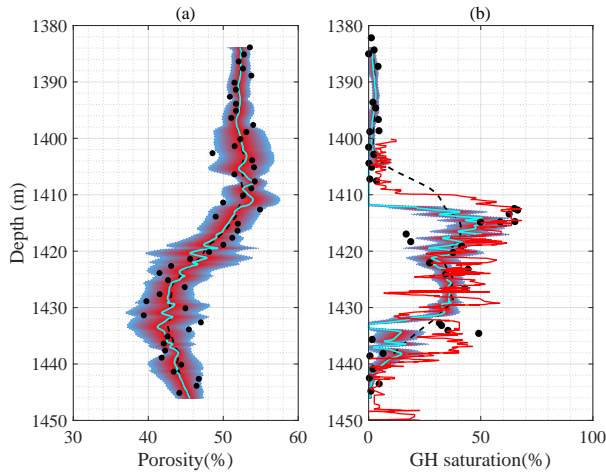
Herein, in the actual inversion process, prior information of the GH saturation and porosity was introduced in the estimation. The probability distribution functions of the prior models were obtained by statistically analyzing the information independent of the observed data, which have an important impact on the estimation results. Different prior models were used in our study to examine their impact on the estimation results. Given that the porosity changes slightly with depth and the inversion result of porosity was good, the prior model of porosity was kept consistent with the previous text, while the prior model for GH saturation was modified. Fig. 5 displays three different prior GH saturation models for the purposes of inversion testing.

Table 2 lists the MSD of the prior and posterior models for different GH saturations, along with the MSE of the inversion results. Fig. 6 illustrates the GH saturation inversion results using the three prior saturation models. It can be observed that prior model 2 displays the highest MSD and deviates significantly from the reference value. Consequently, its estimated saturation of GH has the largest MSE and posterior MSD. Both prior model 1 and model 3 are close to the reference values and have lower prior MSD. Therefore, the estimation results using prior model 1 and model 3 have higher accuracy and lower uncertainty.

It is worth noting that the uncertainties of the inversion results are affected by several factors. First, they are influenced by the accuracy of the physical model. Although the linearized equation can be solved quickly, sometimes it does not represent an accurate petrophysical relationship. However, a numerical optimization of the linear approximation can be



**Fig. 3.** Well log data and GH saturation curves of well W19. (a) Sonic P-wave velocity, (b) density, (c) resistivity, (d) density porosity, (e) the red dots denote the GH saturation estimated by the pore water chemistry and the black line indicates linear interpolation.



**Fig. 4.** Estimation results of (a) porosity and (b) GH saturation. The black dots denote the reference values, the black botted lines denote the prior models, and the bright blue curves indicate the MAP solutions. The shaded area means 95% confidence interval and the red line is GH saturation calculated by the Simandoux model.

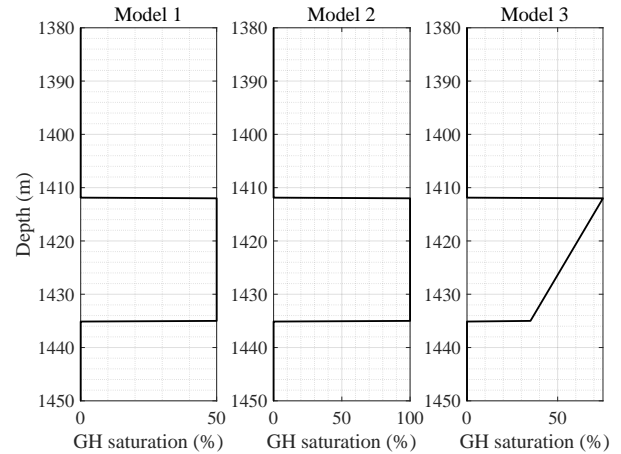


**Fig. 5.** GH saturation prior models.

applied in linear inversion, which can also impact the inversion results. In summary, more accurate petrophysical models and high-quality data can help to obtain more accurate inversion results while reducing the level of uncertainty.

#### 4.2 Sensitivity of data from different sources

performed to enhance the accuracy of the physical model, as exemplified by the earlier mentioned optimization of the linearized Archie’s equation. Second, the noise in the real data also causes uncertainty. Third, to ensure the stability of numerical calculation, varying regularization techniques are

Different data sources may have different data-fitting errors. Therefore, it is crucial to conduct sensitivity analysis on the observational data and the model parameters. Fig. 7 illustrates the relative changes (RC) in density, velocity and resistivity computed using Eqs. (4), (5), and (10) under given

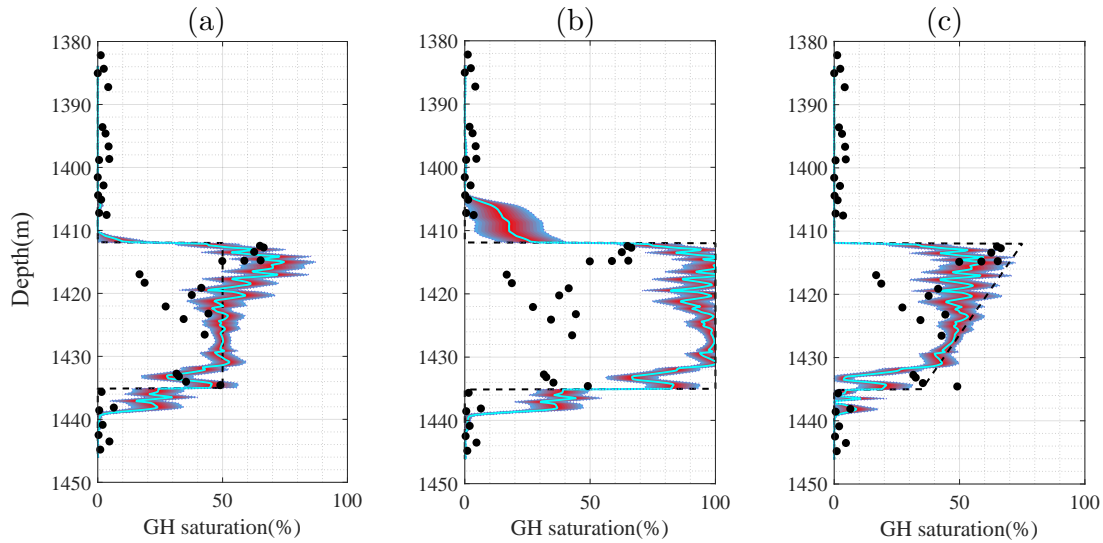


**Fig. 6.** Inversion results for GH saturation prior (a) model 1, (b) model 2 and (c) model 3.

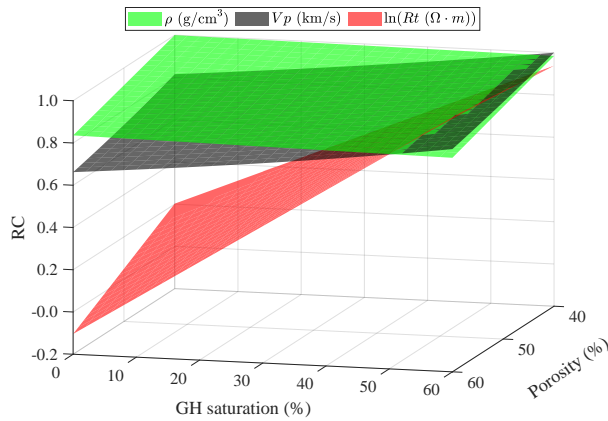


**Fig. 7.** The relative changes in density, velocity and resistivity vary with GH saturation and porosity.

range of reservoir porosity and GH saturation. The RC represent those of the computed density, velocity and resistivity values divided by their respective maximum values, while its value cannot exceed 1. It is essential to emphasize that, given the use of the natural logarithms of resistivity values during the inversion process, sensitivity analysis is also performed using the natural logarithms of resistivity values in the calculations. From Fig. 7, it can be observed that resistivity exhibits the most significant change, followed by velocity, while density shows the weakest change. Combining these observations with Figs. 8(a) and 8(b), it is evident that density is not sensitive to change in GH saturation. This can be attributed to the close densities of water and GH, consistent with the previously discussed perspective. In contrast, resistivity is more sensitive to change in GH saturation than porosity. It is also apparent that as GH saturation increases, resistivity is less sensitive to porosity, and in cases where the GH saturation is 54%, an increase in porosity even leads to an increase in resistivity. This is because GHs are poor conductors of electricity, and at high saturation, an increase in porosity does not enhance the

conductivity of the formation.

The covariance matrix can measure the degree of correlation or linear relationships between multiple random variables. Therefore, when performing joint inversion with multiple data sources, calculating the covariance matrix of different data sources allows us to understand the degree of correlation and the individual distribution characteristics among various data. This in turn provides a reference for developing joint inversion algorithms in subsequent steps. Eq. (18) displays the covariance matrix between the computed density, velocity and resistivity. The parameters  $\sigma_\rho$ ,  $\sigma_{V_p}$  and  $\sigma_{\ln R_t}$  represent the standard deviation of density, velocity and resistivity, respectively. The parameter  $\tau_1$  represents the correlation coefficient between velocity and density,  $\tau_2$  represents the correlation coefficient between density and resistivity, and  $\tau_3$  represents the correlation coefficient between velocity and resistivity. For this case, the non-diagonal part of the matrix represents the covariance between the different data. A higher variance implies that data within the specified range of reservoir porosity and GH saturation shows more pronounced fluctuations, indicating greater sensitivity to changes in porosity and GH saturation. Meanwhile, an increased covariance signifies a stronger relationship between two sets of data. It can be observed that resistivity exhibits the highest variance, followed by velocity, while density has the lowest variance. This pattern aligns with the observations shown in Figs. 7 and 8.

$$\begin{aligned}
 C_d &= \begin{bmatrix} \sigma_\rho^2 & \tau_1 \sigma_\rho \sigma_{V_p} & \tau_2 \sigma_\rho \sigma_{\ln R_t} \\ \tau_1 \sigma_\rho \sigma_{V_p} & \sigma_{V_p}^2 & \tau_3 \sigma_{V_p} \sigma_{\ln R_t} \\ \tau_2 \sigma_\rho \sigma_{\ln R_t} & \tau_3 \sigma_{V_p} \sigma_{\ln R_t} & \sigma_{\ln R_t}^2 \end{bmatrix} \\
 &= \begin{bmatrix} 0.0110 & 0.0128 & 0.0011 \\ 0.0128 & 0.0514 & 0.0983 \\ 0.0011 & 0.0983 & 0.2616 \end{bmatrix}
 \end{aligned} \quad (18)$$

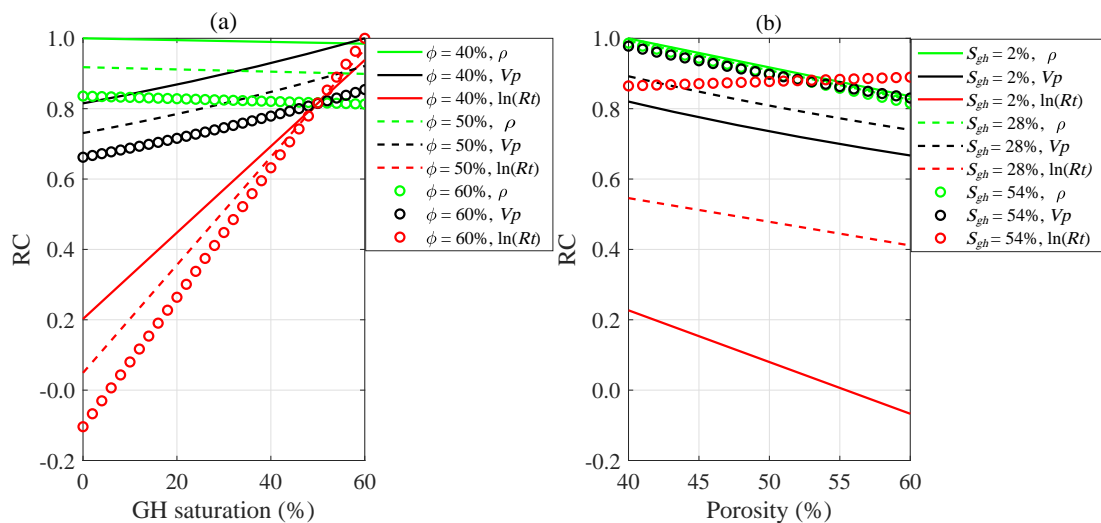


**Fig. 8.** The relative changes in density, velocity and resistivity vary with GH saturation and porosity.

In the Bayesian framework, the likelihood function incorporates the covariance matrix of the observed data into the solution of the inverse problem. The covariance matrix of different data sources can balance their misfit, which matches well with the inherent consistency of solving inverse problems using the weighted least squares method (Zhdanov, 2015). In other words, the covariance matrix can be viewed as a matrix of weighting coefficients or sensitivity factors for different data sources. This property enhances the robustness and accuracy of the joint inversion.

## 5. Conclusions

For GH reservoir characterization, it is a common method to estimate reservoir porosity and GH saturation by using sonic wave velocity, density or resistivity. Due to the complex distribution of GH in the reservoir, it is challenging to accurately estimate the GH reservoir parameters from a single type of data, such as velocity, density or resistivity. This study involves estimating GH saturation and porosity within a linear Bayesian framework by integrating well log data on sonic wave velocity, density and resistivity. A real well log data example is used to demonstrate that this method can not only provide a quick estimation of GH reservoir parameters but also improve the accuracy and reduce the uncertainty of reservoir parameters estimation. In future research considering the effect of the microscopic distribution of GH on the velocity, density and resistivity, different petrophysical models should be selected for the estimation of GH reservoir parameters.

## Acknowledgements

This work was supported by National Natural Science Foundation of China (No. U20B6005), the Shanghai Science and Technology Innovation Plan (No. 21DZ2207000), and the Fundamental Research Funds for the Central Universities.

## Conflict of interest

The authors declare no competing interest.

**Open Access** This article is distributed under the terms and conditions of the Creative Commons Attribution (CC BY-NC-ND) license, which permits unrestricted use, distribution, and reproduction in any medium, provided the original work is properly cited.

## References

- Archie, G. E. The electrical resistivity log as an aid in determining some reservoir characteristics. *Transactions of the AIME*, 1942, 146(1): 54-62.
- Bosch, M., Mukerji, T., Gonzalez, E. F. Seismic inversion for reservoir properties combining statistical rock physics and geostatistics: A review. *Geophysics*, 2010, 75(5): 75A165-75A176.
- Boswell, R. Natural gas-hydrates: Status of potential as an energy resource, in *Future Energy*, edited by R. Boswell, S. Hancock, K., Yamamoto, et al., Elsevier, Amsterdam, pp. 111-131, 2020.
- Brugada, J., Cheng, Y., Soga, K., et al. Discrete element modelling of geomechanical behaviour of methane hydrate soils with pore-filling hydrate distribution. *Granular Matter*, 2010, 12: 517-525.
- Cai, J., Wei, W., Hu, X., et al. Electrical conductivity models in saturated porous media: A review. *Earth-Science Reviews*, 2017, 171: 419-433.
- Chand, S., Minshull, T. A., Gei, D., et al. Elastic velocity models for gas-hydrate-bearing sediments—a comparison. *Geophysical Journal International*, 2004, 159(2): 573-590.
- Chong, Z., Yang, S., Babu, P., et al. Review of natural gas hydrates as an energy resource: Prospects and challenges. *Applied Energy*, 2016, 162: 1633-1652.
- Collett, T. S., Bahk, J. J., Baker, R., et al. Methane hydrates in nature current knowledge and challenges. *Journal of Chemical & Engineering Data*, 2015, 60(2): 319-329.
- Cook, A. E., Waite, W. F. Archie's saturation exponent for natural gas hydrate in coarse-grained reservoirs. *Journal of Geophysical Research: Solid Earth*, 2018, 123(3): 2069-2089.

- Dai, J., Xu, H., Snyder, F., et al. Detection and estimation of gas-hydrates using rock physics and seismic inversion: Examples from the northern deepwater Gulf of Mexico. *The Leading Edge*, 2004, 23(1): 60-66.
- Dvorkin, J., Prasad, M., Sakai, A., et al. Elasticity of marine sediments: Rock physics modeling. *Geophysical Research Letters*, 1999, 26(12): 1781-1784.
- Helgerud, M. B., Dvorkin, J., Nur, A., et al. Elastic-wave velocity in marine sediments with gas-hydrates: Effective medium modeling. *Geophysical Research Letters*, 1999, 26(13): 2021-2024.
- Jin, Y., Li, S., Yang, D. Experimental and theoretical quantification of the relationship between electrical resistivity and hydrate saturation in porous media. *Fuel*, 2020, 269: 117378.
- Kang, D., Xie, Y., Lu, J., et al. Assessment of natural gas-hydrate reservoirs at Site GMGS3-W19 in the Shenhu area, South China Sea based on various well logs. *China Geology*, 2022, 5(3): 383-392.
- Lawrence, M. A., David, R. C. Characterization and analysis of porosity and pore structures. *Reviews in Mineralogy and Geochemistry*, 2015, 80 (1): 61-164.
- Lee, M. W., Hutchinson, D. R., Collett, T. S., et al. Seismic velocities for hydrate-bearing sediments using weighted equation. *Journal of Geophysical Research: Solid Earth*, 1996, 101(B9): 20347-20358.
- Lee, M. W., Collett, T. S. Elastic properties of gas-hydrate-bearing sediments. *Geophysics*, 2001, 66(3): 763-771.
- Li, J., Ye, J., Qin, X., et al. The first offshore natural gas-hydrate production test in South China Sea. *China Geology*, 2018, 1(1): 5-16.
- Li, C., Zhao, Q., Xu, H., et al. Relation between relative permeability and hydrate saturation in Shenhu area, South China Sea. *Applied Geophysics*, 2014, 11: 207-214.
- Mavko, G., Mukerji, T., Dvorkin, J. *The Rock Physics Handbook*. Cambridge, UK, Cambridge University Press, 2020.
- Michelle, A. K., Kyle, P., Danielle, O. Lithology dependence of porosity in slope and deep marine sediments. *Journal of Sedimentary Research*, 2011, 81(10): 730-742.
- Qian, J., Wang, X., Collett, T. S., et al. Downhole log evidence for the coexistence of structure II gas hydrate and free gas below the bottom simulating reflector in the South China Sea. *Marine and Petroleum Geology*, 2018, 98: 662-674.
- Shankar, U., Riedel, M. Gas hydrate saturation in the Krishna-Godavari basin from P-wave velocity and electrical resistivity logs. *Marine and Petroleum Geology*, 2011, 28(10): 1768-1778.
- Simandoux, P. Dielectric measurements in porous media and application to shaly formation: *Revue de l'Institut Français du Pétrole*. Supplementary Issue, 1963, 18: 193-215.
- Sun, J., Zhang, L., Ning, F., et al. Production potential and stability of hydrate-bearing sediments at the site GMGS3-W19 in the South China Sea: A preliminary feasibility study. *Marine and Petroleum Geology*, 2017, 86: 447-473.
- Tarantola, A. *Inverse Problem Theory and Methods for Model Parameter Estimation*. Philadelphia, USA, Society for Industrial and Applied Mathematics, 2005.
- Trofimuk, A. A., Cherskiy, N. V., Tsarev, V. P. The reserves of biogenic methane in the ocean. *Doklady Akademii nauk SSSR*, 1975, 225: 936-939.
- Wang, X., Collett, T. S., Lee, M. W., et al. Geological controls on the occurrence of gas hydrate from core, downhole log, and seismic data in the Shenhu area, South China Sea. *Marine Geology*, 2014, 357: 272-292.
- Wood, W. T., Stoffa, P. L., Shipley, T. H. Quantitative detection of methane hydrate through high-resolution seismic velocity analysis. *Journal of Geophysical Research: Solid Earth*, 1994, 99(B5): 9681-9695.
- Wyllie, M. R. J., Gregory, A. R., Gardner, L. W. Elastic wave velocities in heterogeneous and porous media. *Geophysics*, 1956, 21(1): 41-70.
- Yang, S., Liang, J., Lu, J., et al. New understandings on the characteristics and controlling factors of gas hydrate reservoirs in the Shenhu area on the northern slope of the South China Sea. *Earth Science Frontiers*, 2017, 24(4): 1-14. (in Chinese)
- Ye, J., Qin, X., Xie, W., et al. The second natural gas-hydrate production test in the South China Sea. *China Geology*, 2020, 3(2): 197-209.
- Yu, T., Guan, G., Abudula, A. Production performance and numerical investigation of the 2017 offshore methane hydrate production test in the Nankai Trough of Japan. *Applied Energy*, 2019, 251: 113338.
- Yun, T. S., Francisca, F. M., Santamarina, J. C., et al. Compressional and shear wave velocities in uncemented sediment containing gas hydrate. *Geophysical Research Letters*, 2005, 32(10): L10609.
- Zhdanov, M. S. *Inverse Theory and Applications in Geophysics*. Amsterdam, NL, Elsevier, 2015.